JOURNAL OF Materials CHEMISTRY

Synthesis and crystal structure of the distorted perovskite $Sr_{0.97}NbO_3$ determined by high resolution powder neutron diffraction

Nianhua Peng,[a] John T. S. Irvine[a] and Alexander G. Fitzgerald,[b]

[a]*School of Chemistry, University of St. Andrews, St. Andrews, UK KY16 9ST*
[b]*Department of Applied Physics and Electronic & Manufacturing Engineering, University of Dundee, Dundee, UK DD1 4HN*

A new perovskite related $Sr_{0.97}NbO_3$ phase has been synthesized. Although both powder X-ray diffraction and selected area electron diffraction studies suggest a primitive cubic perovskite structure with $a_p \approx 4.023$ Å, high resolution powder neutron diffraction reveals a subtle lattice distortion from cubic symmetry. The detailed crystal structure has been refined with the orthorhombic space group $P2_12_12$ with $a = 5.6881$ Å, $b = 5.6821$ Å and $c = 8.0566$ Å. The structure is built up from two types of NbO_6 octahedra, one elongated, the other compressed along c. The lattice distortion from cubic symmetry has been found to mainly originate from tilting of NbO_6 octahedra, whereas the $\sqrt{2}a_p \times \sqrt{2}a_p \times 2a_p$ superstructure arises from ordering of alternate elongated and compressed octahedra.

Introduction

Early attempts at the preparation of an ideal $SrNbO_3$ perovskite compound in vacuum at high temperature ended without success.[1–3] A simple cubic perovskite structure has been identified by X-ray diffraction studies in Sr site deficient $Sr_{1-x}NbO_3$ compounds, where $0.05 \leqslant x \leqslant 0.25$. As part of our investigations of the ternary SrO–NbO–Nb_2O_5 system in flowing Ar gas atmosphere, we have succeeded in forming single phase $Sr_{1-x}NbO_3$ materials with low Sr site deficiencies. By pushing the x value even closer to the zero point, a simple cubic perovskite structure with $a_p = 4.023(1)$ Å can be derived from both powder X-ray and selected area electron diffraction data for an $Sr_{0.97}NbO_3$ sample; however, non-cubic distortion of the crystal structure has been revealed in a high resolution neutron powder diffraction study. This distortion leads to the formation of an orthorhombic unit cell. The details of this study are described below.

Experimental

Samples with starting stoichiometric composition '$SrNbO_3$' were prepared by solid state reaction at high temperature in flowing Ar gas atmosphere. Our early experimental work has demonstrated the advantage of this approach over the more conventional sample preparation method in vacuum for the formation of reduced transition metal oxide compounds.[4,5] A $Sr_4Nb_2O_9$ precursor was prepared by grinding $SrCO_3$ and Nb_2O_5 with acetone and firing at 1200 °C for about 48 h with intermediate grindings. The '$SrNbO_3$' was then prepared from an appropriate mixture of $Sr_4Nb_2O_9$, Nb and Nb_2O_5 powders. The mixture was ground in an agate mortar and pestle in acetone for more than 30 min, then pressed into a pellet with a 13 mm diameter die, and slowly heated to 1400 °C. After high temperature reaction for about 10 h, the furnace was cooled at a rate of 10 °C min^{-1}. All $SrCO_3$, Nb and Nb_2O_5 were commercially available 99.9% pure powders.

Phase formation was monitored closely by powder X-ray diffraction. All powder X-ray diffraction data were collected on a STÖE diffractometer fitted with Cu-Kα radiation and position sensitive detectors in transmission mode and Philips diffractometer in reflection mode. The samples were also examined using selected area electron diffraction with a JEOL 100 CX TEM. Low temperature ac electrical resistance was measured on sintered pellets by the standard four lead technique. Silver paste was used to attach copper leads onto the sample. An Oxford Instruments top loading compact variable temperature insert was used to cool the sample to 2.6 K in a liquid He dewar. Temperature was measured using a RhFe sensor, and controlled by an Oxford Instruments ITC503 temperature controller. The ac current amplitude was about 10 mA, $f = 333.3$ Hz. The ac voltage drop on the sample was measured by a Stanford SR830 lock-in amplifier. Magnetic susceptibility has been measured at low temperature by an Oxford Instruments VSM, the applied magnetic field was 100 G. The overall chemical stoichiometry, in particular the oxygen content or the oxidation state of transition metal ions, was analyzed by a TA Instrument TGA under flowing oxygen conditions from room temperature to 1200 °C at a rate of 10 °C min^{-1}. High resolution neutron powder diffraction data were collected at the ISIS HRPD station of the Rutherford-Appleton Laboratory at room temperature. The resolution ($\Delta d/d$) is better than 0.0005. The powder samples were contained in a cylindrical holder made of vanadium. The diffraction data were refined in the time-of-flight range between 35 000 μs and 110 000 μs with $2\theta = 168.329°$ by the Rietveld method,[6,7] using the program TF12LS.[8] Neutron scattering lengths of 0.7054×10^{-12} cm for Nb, 0.702×10^{-12} cm for Sr and 0.5803×10^{-12} cm for O were used.[9]

Space group determination and Rietveld refinement of HRPD data

Determination of unit cell dimension and construction of starting structure model for Rietveld refinement

The high resolution neutron diffraction pattern is shown in Fig. 1, and the d-spacings for those diffraction lines greater than 1.2 Å are also listed in Table 1. As both the powder X-ray diffraction pattern and the selected area electron diffraction pattern can be easily indexed as a simple cubic perovskite structure with $a_p = 4.023(1)$ Å, an attempt was made to index all observed diffraction peaks with a simple pseudo-cubic unit cell first. Interestingly, calculated a_p^2/d^2 values clearly show the non-cubic distortion and enlargement of the pseudo-cubic cell, as tabulated in Table 1.

Firstly, the splitting of some strong diffraction lines, such as the $d = 2.0148$ Å and $d = 2.0106$ Å peaks as shown in Fig. 2(a), is not expected for a single cubic phase, although their calculated a_p^2/d^2 ratios are very close to an integer value. Secondly,

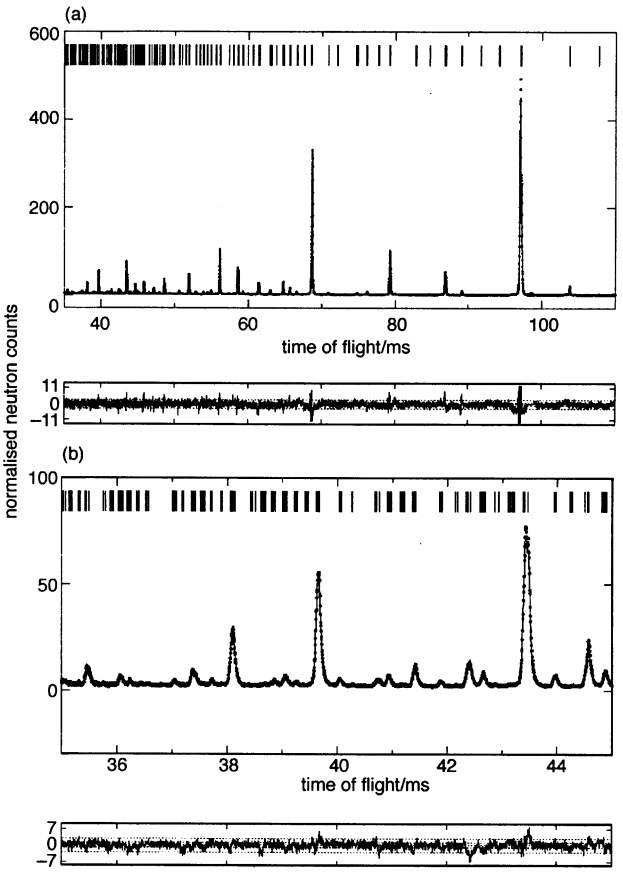

Fig. 1 (a) Room temperature time-of-flight powder neutron diffraction pattern of $Sr_{0.97}NbO_3$, dots for experimental raw data and lines for Rietveld refined results with $P2_12_12$ space group, and (b) an enlarged section of the above diffraction pattern

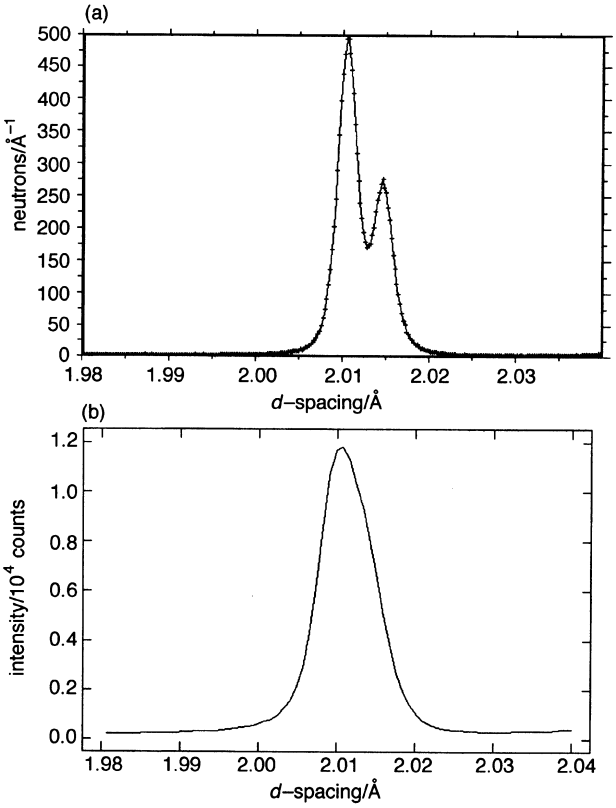

Fig. 2 (a) Enlarged neutron diffraction pattern showing (220) and (004) splitting and (b) corresponding diffraction peaks of (220) and (004) planes by powder X-ray diffraction, showing the asymmetric peak shape only

Table 1 Observed neutron powder diffraction peak positions ($d > 1.5$ Å) and their intensities (a_p is the cubic unit cell edge calculated from XRD. If a_p/d has an integer value then this reflection can be indexed on a simple cubic cell and if it has a fractional value it can be indexed on an ordered cubic cell; however, if the cell is distorted from cubic symmetry the value of a_p/d will not correspond to a simple fraction)

d/Å	I_{obs}	I_{rel}	a_p^2/d^2 (rounded value)
2.4288	25	5.1	2.744 (2¾)
2.4252	18	3.6	2.752 (2¾)
2.3232	488	98.6	2.999 (3)
2.1509	22	4.4	3.498 (3½)
2.0420	7	1.4	impurity
2.0148	278	56.2	3.987 (4)
2.0106	495	100	4.004 (4)
1.8468	11	2.2	4.745 (4¾)
1.80123	42	8.5	4.988 (5)
1.79898	54	10.9	5.001 (5)
1.64283	103	20.8	5.997 (6)
1.57921	8	1.6	6.490 (6½)
1.55078	5	1.0	6.730 (6¾)
1.54799	5	1.0	6.754 (6¾)
1.46884	7	1.4	7.502 (7½)
1.42321	332	67.1	7.990 (8)
1.37962	10	2.0	8.503 (8½)
1.36085	19	3.8	8.739 (8¾)
1.34168	30	6.1	8.991 (9)
1.30505	13	2.6	9.503 (9½)
1.27400	25	5.1	9.972 (10)
1.27191	28	5.7	10.004 (10)
1.24213	6	1.2	10.490 (10½)
1.22808	10	2.0	10.731 (10¾)
1.21439	60	12.1	10.975 (11)
1.21294	65	13.1	11.001 (11)

many weak extra peaks are not observed by either powder X-ray diffraction or electron diffraction studies. The appearance of remnants like 1/2 and 3/4 in their a_p^2/d^2 ratios clearly shows that the real unit cell dimensions should be at least four times bigger than the simple pseudo-cubic cell derived from the powder X-ray diffraction and selected area electron diffraction data, if all diffraction peaks are to be indexed with integer Miller index *hkls*. In fact, all observed *d*-spacings can be indexed very well with a quasi-tetragonal cell with $a = b = 5.6852(1)$ Å and $c = 8.0563(2)$ Å, except for a weak impurity peak with $d = 2.0420$ Å.

The construction of a starting crystal structure for Rietveld refinement is based on the Fourier mapping of experimental diffraction data, in which the density of electronic charges can be plotted out, and combined with previous studies on $Sr_{1-x}NbO_3$ samples by single crystal X-ray diffraction.[10] It is reasonable to assume that the unit cell concerned here is a four times enlargement of the simple cubic perovskite cell with $a = b \approx \sqrt{2}a_p$, and $c \approx 2a_p$, where a_p is the lattice parameter of an ideal perovskite cubic cell. Consequently, the starting atomic positions have been derived, as listed in Table 2. Here the Sr atoms are on the corner A sites, Nb atoms occupy the central octahedral B sites and all oxygens are in the face-centre positions in the original perovskite framework. Site displacements can be introduced in accordance with the space group used for the refinement.

Table 2 Starting fractional positions of component atoms in an enlarged ideal perovskite cell

atom	fractional positions xyz
Sr	000, ½½½, 00½, ½½0
Nb	½0¼, 0½¼, ½0¾, 0½¾
O	¼¼¼, ¾¾¾, ¾¾¼, ¾¼¼, ¼¼¾, ¼¾¾, ¾¼¾, ¼¾¼, ½00, 0½0, ½0½, 0½½

Attempted refinement with a tetragonal symmetry space group

As the observed *d*-spacings can be indexed satisfactorily with a tetragonal unit cell, Rietveld refinement of the diffraction profile with a tetragonal space group was carried out first. Refinements with space group $P\bar{4}2_1c$ (no. 114), $P4_2mc$ (no. 105), $P\bar{4}2c$ (no. 112), $P4_2/mmm$ (no. 131) and $P4/nnc$ (no. 126) were examined. All of them failed to give a satisfactory fitting for the experimental diffraction profile, and the refinements did not converge to an acceptable level.

The poor fitting of experimentally observed neutron diffraction data by any tetragonal space group mentioned so far is mainly due to the presence of significant diffraction intensities for some peaks which should be very weak if the space group was tetragonal; a typical example is shown in Fig. 3(a). For space group $P\bar{4}2_1c$, the calculated diffraction intensity for the observed (105) diffraction peak is insignificant, whereas the calculated neighbouring (321) and (303) combined diffraction peak intensity is larger than that observed experimentally.

Refinement of experimental data with orthorhombic symmetry space groups

The failure to refine the diffraction profile with a tetragonal space group suggests that orthorhombic lattice symmetry might be a better choice. The general conditions of diffraction presence with an orthorhombic lattice are h, k, $l=2n$ for (h00), (0k0) and (00l) diffraction lines respectively. This naturally points to the space group $P2_12_12_1$ (no. 19). However, with only one general position 4a site available, it is apparent that allocation of all component atoms into the 4a site has changed the perovskite based structure quite significantly. As restricted by the symmetry operations, it is hard to allocate atoms into sensible perovskite sites, refinements have been made by varying atomic positions, but all of these failed to reach convergence. This may imply that either the dimension of unit cell adopted so far is not correct or that the prescribed conditions are too strict. Fortunately, for all orthorhombic space groups, there are only five space groups which have less rigorous general conditions, *i.e.*, $P222$ (no. 16), $P222_1$ (no. 17), $P2_12_12$ (no. 18), $Pmm2$ (no. 25) and $Pmmm$ (no. 47). It is possible to refine experimental data using each of these space groups one by one on a trial-and-error approach. Unlike space group $P2_12_12_1$, atom assignments with all these space groups are straightforward without changes in the basic perovskite framework. In Table 3, all refined R factors are listed, the space group $P2_12_12$ (no. 18) clearly gives the lowest residual values (R factors). The detailed refined crystallographic results with space group $P2_12_12$ are summarised in Tables 4, 5 and 6.

Modification of the unit cell dimension has been tried in parallel to the above refinement attempts. For example, similar general conditions like $h=2n$, $k=2n$ and $l=2n$ for (h00), (0k0) and (00l) diffractions can be easily prescribed for a $2a_p \times 2a_p \times 2a_p$ unit cell. All component atoms now can be comfortably assigned into the 4a site with space group $P2_12_12_1$, but the minimum R factors obtained so far are still high (*e.g.*, $R_{wp}=16.5\%$). As we have no direct experimental evidence for the expansion of the unit cell dimension, and more importantly, as the Rietveld refinement with the $P2_12_12$ space group has already resulted in acceptable fitting with a minimum $\sqrt{2}a_p \times \sqrt{2}a_p \times 2a_p$ supercell, it is not necessary to examine further enlarged cell dimensions.

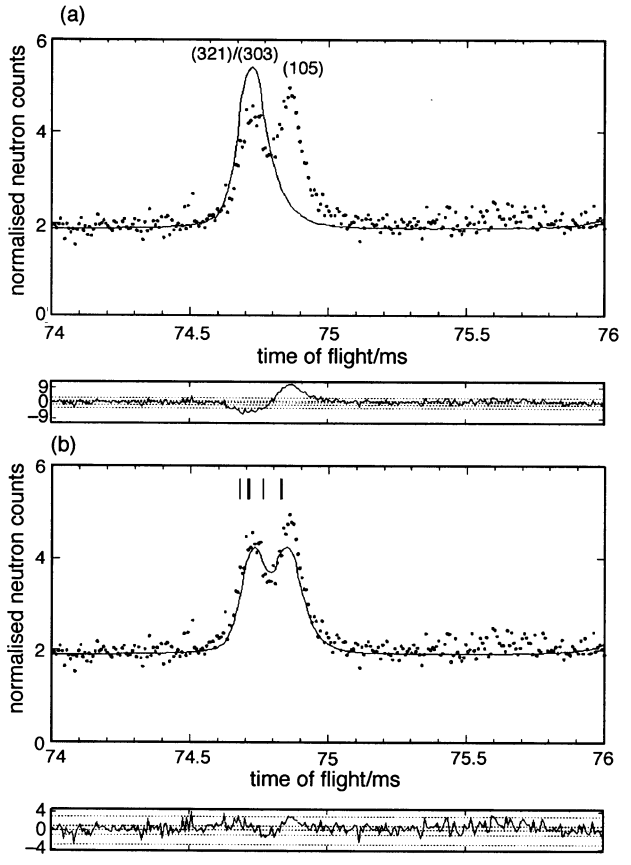

Fig. 3 The difference in profile fitting by using different structural models: (a) poor fitting due to small calculated intensity for the (105) diffraction peak with tetragonal space group $P\bar{4}2_1c$ and (b) improved fitting with orthorhombic space group $P2_12_12$

Table 3 Summary of refined residual factors (R_{wp}) for selected space groups

space group	R_{wp} (%)
$P222$	15.8
$P222_1$	13.4
$P2_12_12$	8.3
$Pmm2$	14.5
$Pmmm$	16.8

Table 4 Refined atomic positions with space group $P2_12_12$

atom	site symmetry	x, y, z	site occupation
Sr1	2a	0.0, 0.0, −0.013(1)	0.99(1)
Sr2	2a	0.0, 0.0, 0.514(1)	0.95(1)
Nb1	2b	0.0, 0.5, 0.751(1)	1.0
Nb2	2b	0.0, 0.5, 0.249(1)	1.0
O1	4c	0.256(1), 0.263(1), 0.245(1)	1.0
O2	4c	0.715(1), 0.722(1), 0.740(1)	1.0
O3	2b	0.5, 0.0, 0.006(1)	1.0
O4	2b	0.0, 0.5, 0.506(1)	1.0

Table 5 Refined lattice parameters and temperature factors

$a=5.68807(1)$ Å	space group $P2_12_12$, no. 18
$b=5.68214(1)$ Å	limit of TOF: 35000–110000 μs
$c=8.05658(1)$ Å	$R_p=5.8\%$
$V=260.392(1)$ Å^3	$R_{wp}=8.3\%$
$Z=4$	$R_{exp}=4.7\%$

atom	B_{11}	B_{22}	B_{33}	B_{23}	B_{13}	B_{12}
Sr1	0.54(4)	0.54(4)	0.54(4)	0	0	0
Sr2	0.80(4)	0.80(4)	0.80(4)	0	0	0
Nb1	0.61(4)	0.61(4)	0.61(4)	0	0	0
Nb2	0.59(4)	0.59(4)	0.59(4)	0	0	0
O1	1.61(8)	0.81(7)	2.73(7)	0.0(2)	0.4(2)	1.05(4)
O2	0.60(2)	0.60(2)	0.60(2)	0	0	0
O3	2.3(2)	2.1(2)	0.25(7)	0	0	0.8(2)
O4	0.80(5)	0.80(5)	0.80(5)	0	0	0

Table 6 Bond lengths and angles refined from high resolution neutron diffraction data

bond length/Å		bond angle/°	
Nb1—O1	2.037(1)	O1—Nb1—O1	178.0(1)
Nb1—O2	2.058(1)	O1—Nb1—O2	85.06(5)
Nb1—O3	1.957(1)	O1—Nb1—O3	89.01(5)
Nb1—O4	1.974(1)	O1—Nb1—O4	90.99(5)
		O2—Nb1—O2	174.8(1)
		O2—Nb1—O3	92.57(5)
		O2—Nb1—O4	87.43(5)
		O3—Nb1—O4	179.9(1)
Nb2—O1	1.986(1)	O1—Nb2—O1	177.6(1)
Nb2—O2	1.997(1)	O1—Nb2—O2	85.02(5)
Nb2—O3	2.061(1)	O1—Nb2—O3	88.80(5)
Nb2—O4	2.062(1)	O1—Nb2—O4	91.20(5)
		O2—Nb2—O2	175.1(1)
		O2—Nb2—O3	92.47(5)
		O2—Nb2—O4	87.53(5)
		O3—Nb2—O4	179.9(1)

Discussion

The well defined diffraction peak splitting of the (220) and (004) planes displayed in Fig. 2(a) clearly shows the advantage of a high resolution neutron diffraction study over conventional powder X-ray diffraction, in which only one relatively broad diffraction peak can be observed, as the difference in 2θ diffraction angle is about 0.1° for (220) and (004) diffraction planes, as shown in Fig. 2(b). The small difference in the *a* and *b* lattice parameters agrees well with the quasi-tetragonal nature of the lattice symmetry, as a survey of all diffraction peaks does not reveal any direct evidence for the splitting of those (*hkl*) and (*khl*) diffraction peaks. Compared to the obvious off-site movements of oxygen anions, shifts of cation coordinates are moderate; in particular such shifts for the Nb ions are very small (Table 4), suggesting that the heavy metal framework adopts a more or less rigid cubic-like structure, consistent with the X-ray and electron diffraction results. In fact, by using the structural model refined from neutron data, a simple cubic-like powder X-ray diffraction pattern can be easily simulated. Selected area electron diffraction did not reveal any direct evidence for the formation of an enlarged unit cell.

The principal cause of the distortion from cubic symmetry lies in the anion sub-lattice. The structure is built from two distorted NbO_6 octahedra, one of which ($NblO_6$) is compressed along *c* and the other ($Nb2O_6$) is elongated along *c*, as shown in Fig. 4. These distorted octahedra alternate along [001] ($[001]_p$), [110] ($[100]_p$) and [1$\bar{1}$0] ($[010]_p$) directions giving the $\sqrt{2}a_p \times \sqrt{2}a_p \times 2a_p$ superstructure. As the average Nb—O bond distances are the same (± 0.01 Å) for each of the sets of octahedra, there is no evidence of charge disproportionation at the Nb sites. The buckling of O1—Nb1—O1, O2—Nb1—O2, O1—Nb2—O1 and O2—Nb2—O2 bonds is a direct consequence of off-site movement of oxygens, particularly the O2 site oxygens, as shown in Fig. 4(b). To compensate for the expansion/contraction along *c*, the projected Nb—O bond lengths for both Nb1 and Nb2 sites have been affected differently, which destroys the perfect Nb—O square on the *ab* plane. A projected plot of the crystal structure onto the *ab* plane in Fig. 4(c) shows columns of alternating $Nb1O_6$ and $Nb2O_6$ octahedra along *c*, with adjoining columns tilted antiphase.

The *R* factors, in particular R_{exp}, as listed in Table 5, obtained so far are relatively high for Rietveld refinement of powder neutron diffraction data. In order to keep the high resolution of the neutron diffraction data, which is vital to our studies here, we did not bin the experimental data points for our refinement, in contrast to the normal approach widely used for the neutron data refinement. Binning of data points greatly reduces the contribution of noise to the collected data and so decreases the residual values. To compare the difference between experimental data with binning and without binning, we tried to bin experimental data for every five experimental points; this led to a decrease in all *R* factors by about a fifth in magnitude. Such a binning process will impair resolution, particularly for peaks showing splitting of diffraction peaks with small Δd, as illustrated in Fig. 2(a).

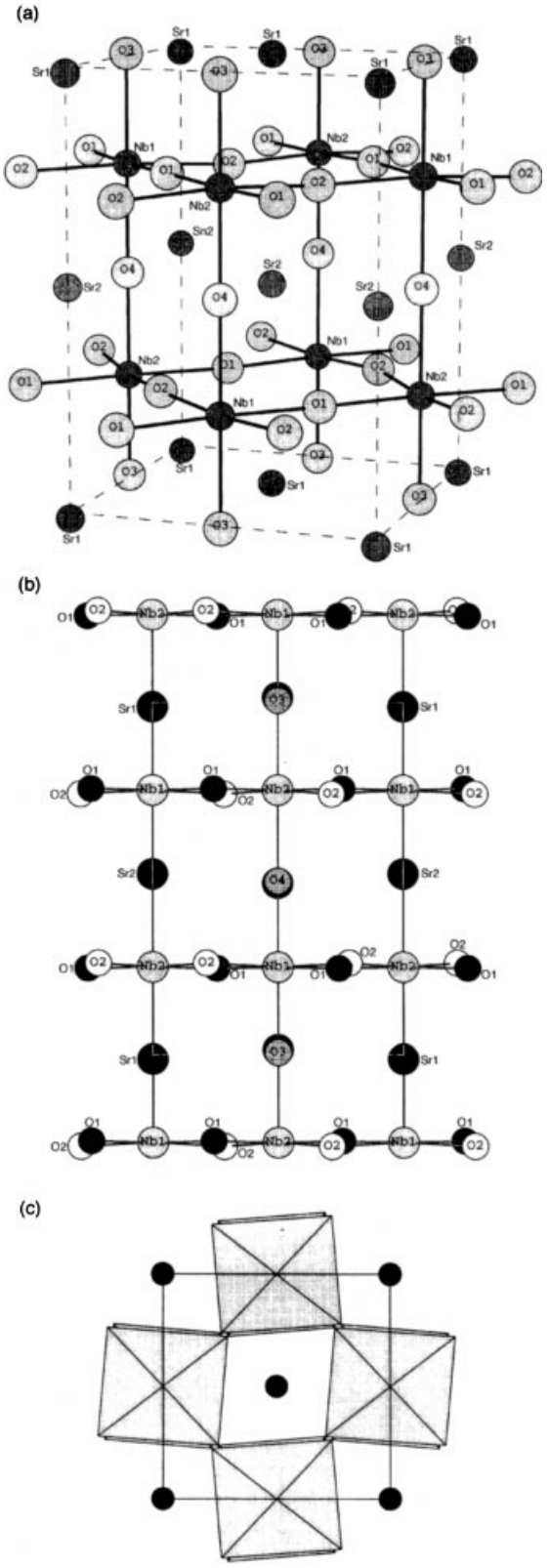

Fig. 4 (a) Refined crystal structure of $Sr_{0.97}NbO_3$ with labels of component atoms, (b) projection of the unit cell along the *b* direction, and (c) projection of the unit cell along the *c* direction

The value of the quasi-cubic lattice parameter a_p indicates a very low Sr site vacancy concentration level, $x=0.02(2)$, when compared to various $Sr_{1-x}NbO_3$ samples reported previously.[1,3] Neutron diffraction data refinement gives the overall chemical composition of this sample as $Sr_{0.97}NbO_3$ ($\Delta x<0.01$), consistent with the result estimated from the lattice parameter derived from powder X-ray diffraction data. Both of these are consistent with the TGA result too, as shown in Fig. 5. The weight gain (about 3.5%) after firing $Sr_{0.97}NbO_3$ in O_2 is in accord with the value expected for oxidation of all Nb^{4+} ions into Nb^{5+} ions. The powder X-ray diffraction pattern of the oxidised product can be indexed as $Sr_2Nb_2O_7$. The slight Sr deficiency can be explained by a mass loss at high reaction temperature. Such a process is moderate for the experimental conditions applied in the sample preparation. More serious mass loss has been recorded upon extended firing at high temperature with a fast flow rate of inert gas, or upon firing at high temperature in vacuum.

Previous crystal structural studies on the Sr–Nb–O system were mainly based on X-ray diffraction data, so only cation positions could be determined with certainty because of the relatively small X-ray scattering power of oxygen. Some single crystal X-ray diffraction studies performed previously for $Sr_{1-x}NbO_3$ samples ($x=0.28$ and 0.14) have suggested an ideal cubic disordered defect perovskite structure.[10] Only powder X-ray diffraction has been utilised to study samples with smaller x values and for these it would not be surprising that any subtle structural modification involving oxygen would not have been detected, as the contribution to diffraction intensities by such a modification is very weak. The small difference for the neutron scattering length and X-ray scattering amplitude between Sr and Nb makes it very difficult to distinguish between Sr and Nb site occupation with certainty by using the experimental diffraction data directly. However, considering the difference in ionic radii of Nb^{4+} ions and Sr^{2+} ions, *i.e.*, 1.18 Å for Sr^{2+} *versus* 0.69 Å for Nb^{4+} for six-coordinated ions,[11] any Sr and Nb site disordering effect should be reflected from the change in cell parameters for a series of solid state solutions. For perovskite $Sr_{1-x}NbO_3$, cation vacancies at Sr sites can exist over a wide range of compositions. To date there is no report on the ordering or lattice distortion with chemical composition, indicating a random distribution of Sr site vacancies. The situation is different when the A site is occupied by 3+ ions; for example, an ordering of A site vacancies for a perovskite ABO_3 derived structure has been found in $La_{0.33}NbO_3$.[12] It is worth emphasising here again that as far as the distortion of the oxygen anion sublattice is concerned, only neutron diffraction studies can detect the possible complex structure with certainty.

A classification rule proposed by Roth[13] suggests that the ideal $SrNbO_3$ should adopt a pseudo-cubic structure. A large Goldschmidt tolerance factor,[14] $t\approx1$, also implies that it is very unlikely to form an ideal primitive cubic structure with the $SrNbO_3$ composition. Creation of Sr site vacancies can reduce the tolerance factor a little, but its value is still high for a stable simple cubic perovskite structure. Instead a distorted structure is more favourable. Generally speaking, lattice distortion for a perovskite structure can be introduced by cation off-site movement, such as that in ferroelectric $BaTiO_3$,[15] or by the tilting of cation–anion octahedra without significant cation off-site movement, such as that in $CaTiO_3$.[16] As analyzed previously by Glazer,[17] supercell formation resulting from pure tilting of cation–anion octahedra is barely detectable by conventional X-ray diffraction studies. The intensities of supercell diffraction peaks are extremely weak, and can be easily overlooked. $Sr_{1-x}NbO_3$ is just another example belonging to this class of perovskite. It is possible that the lattice distortion described here is a common feature for all $Sr_{1-x}NbO_3$ series, certainly for x values approaching zero. It is worth mentioning here that the intensities of those extra diffractions are still very weak, compared to those fundamental diffraction lines with integer a_p^2/d^2 ratios, even though the scattering powers of cations and oxygen are comparable here. Even weaker intensities should be expected from these diffractions for both X-ray and electron diffraction, where the disparity of scattering powers between anions and cations is greater.

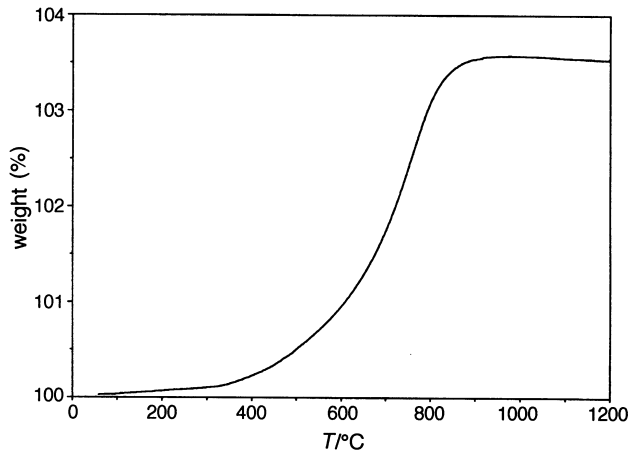

Fig. 5 Thermogravimetric data collected for oxidation of $Sr_{0.97}NbO_3$ sample in flowing O_2 atmosphere

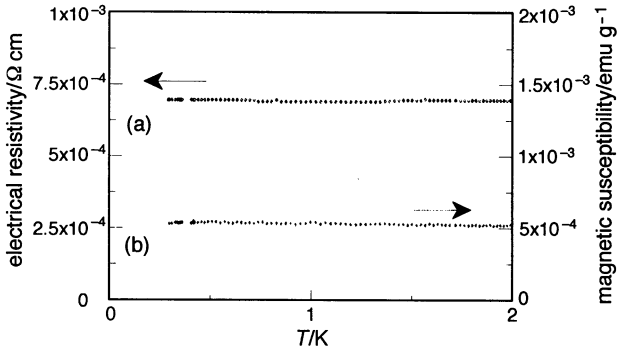

Fig. 6 Temperature independent electrical resistivity (a) and magnetic susceptibility (b) at low temperature

Electrical resistivity was low (*ca.* 0.7 mΩ cm) and independent of temperature between 2.6 K and 300 K, Fig. 6(a). The bulk resistance may well be even lower as samples exhibited low sintered densities (*ca.* 50% theoretical). Magnetic susceptibility was also independent of temperature, Fig. 6(b). Photoacoustic spectrum measurements carried out in the wavelength range from 200 nm to 800 nm show metal-like complete absorption behaviour. This is unusual for an oxide which is dark red in colour.

Conclusion

In summary, by improving sample preparation conditions in a flowing Ar gas atmosphere, a new perovskite related $Sr_{0.97}NbO_3$ compound has been synthesized in this study. The crystal structure of the $Sr_{0.97}NbO_3$ phase has been examined by using powder X-ray diffraction, selected area electron diffraction and high resolution powder neutron diffraction techniques. The simple cubic structure derived from both X-ray and electron diffraction data has been proved to be in disagreement with the neutron diffraction data. Distortion and ordering of NbO_6 octahedra lead to the formation of a $\sqrt{2}a_p\times\sqrt{2}a_p\times2a_p$ supercell. This has been confirmed by the Rietveld refinement of high resolution neutron diffraction data.

We are grateful for the financial support provided by the EPSRC and the Nuffield Foundation. The EPSRC also

provided neutron diffraction facilities at ISIS, Rutherford-Appleton Laboratory. We are grateful to Dr. R. Smith, Mr. R. K. B. Gover and Mr. A. J. Feighery for assistance in the collection of neutron diffraction data. Thanks are due to Prof. R. Cywinski, Mr. R. Stewart and Mr. A. Hillier for assistance in magnetic property measurements.

References

1 D. Ridgley and R. Ward, *J. Am. Chem. Soc*., 1955, **77**, 6132.
2 E. I. Krylov and A. A. Shiarnin, *J. Gen. Chem. USSR*, 1955, **25**, 1637.
3 K. Isawa, J. Sugiyama, K. Matsuura, A. Nozaki and H. Yamauchi, *Phys. Rev. B*, 1993, **47**, 2849.
4 T. J. Cogle, C. A. Mateus, J. H. Binks and J. T. S. Irvine, *J. Mater. Chem*., 1991, **1**, 289.
5 A. B. Sheikh and J. T. S. Irvine, *J. Solid State Chem*., 1993, **103**, 30.
6 H. M. Rietveld, *Acta Crystallogr*., 1967, **22**, 151.
7 H. M. Rietveld, *J. Appl. Crystallogr*., 1969, **2**, 65.
8 W. I. F. David and R. M. Ibberson, Profile Analysis of Neutron Powder Diffraction Data at ISIS, Rutherford-Appleton Laboratory Report RAL-92-032.
9 V. F. Sears, *Neutron News*, 1992, **3**, 26.
10 B. Hessen, S. A. Sunshine, T. Siegrist and R. Jimenez, *Mater. Res. Bull*., 1991, **26**, 85.
11 R. D. Shannon and C. T. Prewitt, *Acta Crystallogr*., *Sect. B*, 1969, **25**, 925.
12 P. N. Iyer and A. J. Smith, *Acta Crystallogr*., 1967, **23**, 740.
13 R. S. Roth, *J. Res. NBS*, 1958, **58**, RP 2736.
14 V. M. Goldschmidt, *Skr. Nor. Vidensk. Akad. Kl. I. Mater. Naturvidensk. Kl*., 1926, **14**, 477.
15 R. W. G. Wyckoff, *Cryst. Struct*., 1964, **2**, 359.
16 H. F. Kay and P. C. Bailey, *Acta Crystallogr*., 1957, **10**, 219.
17 A. M. Glazer, *Acta Crystallogr., Sect B*, 1972, **28**, 3384.

Paper 7/08290H; *Received* 18*th November*, 1997